

UNIVERZITA PALACKÉHO V OLOMOUCI
PŘÍRODOVĚDECKÁ FAKULTA

Katedra optiky



**Optical phase super-resolution at the quantum limit
with coherent and squeezed states of light**

RIGORÓZNÍ PRÁCE

Vypracoval:

Mgr. Miroslav Ježek, Ph.D.

Studijní program:

N1701 / Fyzika

Studijní obor:

1701T029 / Optika a optoelektronika

Abstrakt

Interference světla je důležitým faktorem v mnoha optických aplikacích. Umožňuje přesná interferometrická měření, ale současně omezuje dosažitelné rozlišení. Tato fundamentální vlnově optická limita byla překonána využitím kvantových entanglovaných vícefotonových stavů a nebo komplikovanými neklasickými detekčními metodami. Dosažené superrozlišení je bohužel extrémně citlivé na nedokonalosti detekčního zařízení či optické ztráty samotného měřeného vzorku. Tyto kvantové detekční metody tak vesměs vykazují citlivost horší než prosté intenzitní měření silným optickým signálem. V předložené práci ukážeme, že klasické koherentní stavy světla a běžná koherentní detekce umožňuje superrozlišení s citlivostí škálující se dle $1/\sqrt{N}$, kde N je střední počet fotonů použitého laserového záření. Experimentálně demonstrujeme více než desetinásobné zúžení proužku interferenčního obrazce a superrozlišení dosahující osmi interferenčních proužků připadajících na jednu vlnovou délku. Současně analyzujeme citlivost prezentované metody a její škálování s intenzitou použitého světla. Dále diskutujeme možnost využití stlačeného světla pro interferometrické superrozlišení při současném vylepšení citlivosti pod standardní kvantovou limitu.

Čestné prohlášení

Prohlašuji, že jsem práci napsal samostatně s použitím uvedené literatury.

V Olomouci dne

PALACKY UNIVERSITY OLOMOUC
FACULTY OF SCIENCE

Department of Optics



**Optical phase super-resolution at the quantum limit
with coherent and squeezed states of light**

Miroslav Ježek

2016

Abstract

Interference of light fields plays an important role in various high-precision measurement schemes. It has been shown that super-resolving phase measurements beyond the standard coherent state limit can be obtained either by using maximally entangled multi-particle states of light or using complex detection approaches. In addition to their high technical complexity, these methods lack robustness against imperfections rendering the sensitivity performance above the shot noise limit. Here we show that super-resolving phase measurements at the shot noise limit can be achieved without resorting to non-classical optical states or to low-efficiency detection processes. Using robust coherent states of light, high-efficiency homodyne detection and a deterministic binarization processing technique, we show a narrowing of the interference fringes that scales with $1/\sqrt{N}$ where N is the mean number of photons of the coherent state. Experimentally we demonstrate a more than 10-fold narrowing at the shot noise limit and up to 8 fringes per wavelength. Further, the phase super-resolution technique is extended to squeezed states of light. Preliminary experimental demonstration shows both the super-resolution and super-sensitivity beyond the shot noise limit using solely Gaussian resources—coherent and squeezed states and homodyne tomography.

Keywords

optical phase, super-resolution, sensitivity, coherent state, squeezed state, homodyne detection

Contents

1	Introduction	6
2	Phase super-resolution with classical resources	10
2.1	Theory	10
2.2	Multiple-fringe phase super-resolution	14
2.3	Experimental realization in pulse regime	15
2.4	Experimental results and discussion	16
3	Phase super-resolution beyond shot noise level with coherent and squeezed states	22
3.1	Theory	22
3.2	The ultimate limit of phase sensitivity	25
3.3	Preliminary experimental test in continuous-wave regime	26
4	Conclusion	28

Chapter 1

Introduction

Wave property of light is crucial for many metrological applications as well as in lithography and imaging. A change of a physical quantity coupled to the optical signal can be detected by counting the number of fringes when superimposed with a reference wave. When two coherent electromagnetic waves interfere as in a common Mach-Zehnder interferometer or in Young's double slit experiment, an oscillatory interference pattern arises with a periodicity governed by the wavelength, λ , of the field. The period is given by $\lambda/2$ and is often referred to as the standard resolution limit of interferometers or as the Rayleigh resolution criterion of optical imaging, which represents the minimum resolvable structure in microscopy, lithography, and other applications [1]. Further decreasing the structure size renders the observed feature virtually undetectable. Using a variety of classical image restoration and reconstruction methods the resolution can be partially improved at the expense of excess noise added as for apodization or Fourier deconvolution [2, 3]. Advanced techniques employing tomography synthesis and statistical inference offer several-fold improvement over the Rayleigh limit but they require an excessive data offline processing and do not assure excess noise free operation [4]. Alternatively, approaches based on $4\text{-}\pi$ stimulated emission depletion [5] and other nonlinear interactions were developed to beat the Rayleigh bound by some fixed amount down to the resolution of about 10 nm. Unfortunately, the nonlinear interaction requires high power density of optical radiation which can cause degradation or destruction of the sample. It seems, that the only *scalable* way how to decrease the resolution limit using classical optics is to decrease the wavelength of the light.

Quantum metrology developed in last two decades has overcome the classical Rayleigh limit by exploiting non-classical states of light with the prominent example of multiphoton path entangled states, $(|N, 0\rangle + |0, N\rangle)/\sqrt{2}$, known as NOON states [6, 7]. The effective de Broglie wavelength of NOON state is N times smaller than the optical wavelength of the corresponding unentangled light, which enables *super-resolution*

of phase measurement—that is the resolution beyond the standard $\lambda/2$ limit. Super resolution with NOON states has been demonstrated with ions [8], nuclear spins [9], atoms [10] and photons [11–15]. In addition to the super-resolution, NOON states can in principle also beat the quantum shot noise limit (SNL) in phase estimation ultimately reaching the optimal estimation known as the Heisenberg limit [16]. The SNL yields the sensitivity scaling of $1/\sqrt{N}$, where N is the mean number of photons in the optical signal, whereas for Heisenberg limit it goes as $1/N$. Anything beyond the SNL is called *super-sensitivity*.

Entangled states and especially NOON states with higher number of photons are prepared and detected with very low efficiency [17] and they are extremely susceptible to losses. The probability that NOON state with N photons survives the non-unity transmittance η scales with η^N . As the result of this unfavourable scaling the performance of NOON states decreases and ultimately reaches SNL for N high enough and a sample with arbitrarily low non-zero losses [18]. For losses higher than 79% the sensitivity of phase measurement with NOON states actually decreases for any number $N > 1$ of photons. It is important to stress that the losses are unavoidably implied by the causality. For any physical system the imaginary part of a response function, which causes the absorption, is related to the real part responsible for phase changes induced by the system [19]. It means that only completely lossless vacuum retains the performance of path entangled states better than the SNL for any number of photons but, in this case, there is no phase shift to measure. Carefully engineered entangled states improve the phase measurement performance for intermediate level of losses and low number of photons but this approach converges again to the SNL in the regime of high losses typical for real-life applications [20]. Biological and other interesting samples typically possess a high degree of losses or scattering and non-classical states do not bring us any improvement over the classical strategy. A more promising approach to deterministically beat the SNL (and eventually reaching the Heisenberg Limit) is the one based on single photons in a multiple-pass interferometer with adaptive phase evaluation, although its performance will be ultimately limited by the extended time of flight of the photons [21, 22].

Coherent states of light have also been used to obtain super-resolution. The idea is to detect a nonclassical state (such as the NOON state) via state projection as opposed to nonclassical state preparation [23]. Examples of projections of coherent states that lead to phase super-resolution are photon counting, coincidence counting, and parity detection [15, 24–32]. Although this method largely reduces the complexity of the preparation stage, the detection part remains complex (ideally requiring photon-number-resolving detectors) and the efficiency in projecting out the desired

non-classical state is often very low [26].

A common trait of the presented methods is that their Wigner functions (quasi probability distributions in phase space) associated with the non-classical state preparation or detection are non-Gaussian and negative. Recently, it was realized for Gaussian states that the parity detector could be substituted with a homodyne detector combined with a fast feedback control system [32]. Such features have been shown to be a necessary condition for many quantum information protocols such as entanglement distillation and quantum computing.

For a local phase estimation the super-sensitivity is typically seen as a crucial parameter—an arbitrarily small change of phase response can be, in principle, sensed by the detector if the noise is small enough. It was shown by Caves [33] that the noise can be reduced and the sensitivity of the phase estimation enhanced by injecting a suitable squeezed state of light into the measurement device. Though being nonclassical, the squeezed states belong to Gaussian states together with coherent and thermal states of light. The degradation of squeezed states in the presence of losses is more pronounced than for coherent states but it is not as extreme as for non-Gaussian states with negative Wigner function. Unfortunately, there are only few real-world applications of phase measurement where the sub-SNL sensitivity is actually reached [34–36], or the SNL scaling sensitivity for a broad range of frequencies for that matter. Technical imperfections, such as an excess noise of the detector and discretization of its analog-to-digital converter, obfuscate the signal and render the sensitivity far from the SNL. We can, in this case, improve the phase measurement by increasing the slope of the phase response function. The fundamental quantum noise of the optical signal would stay, of course, the same and the corresponding sensitivity would be increased (worsened) by the same factor. However, this “fundamental” part of the sensitivity would be negligible when compared to the sensitivity penalty due to the dominant classical excess noise.

In this Thesis we discuss a simple and efficient scheme to obtain super-resolution at the SNL without the need of complex nonclassical states in preparation or projectors in detection. We use coherent states of light and a high-efficiency homodyne detector to achieve phase super-resolution beyond what has been achieved with any non-Gaussian resources or detectors. The method is deterministic and we show that it operates close to the shot noise limit. Furthermore, we employ squeezed states of light to improve the sensitivity of super-resolution phase measurement beyond the SNL. We present the detailed theoretical description as well as preliminary experimental demonstration of the measurement.

The first part of the Thesis is based on the work: E. Distante, M. Ježek, and U.L. Andersen, *Deterministic super-resolution with coherent states at the shot noise limit*, Phys. Rev. Lett. 111, 033603 (2013). I undertook this project during my postdoc in the group of prof. U.L. Andersen at Technical University of Denmark in 2009-2010. Simultaneously, I co-supervised the Master's theses *Super-resolution with coherent states* by E. Distante, which was successfully defended at Università degli Studi di Milano in 2011. The theory in the second part of the Theses (squeezed states) has been done by me, the preliminary experimental test was performed by L.S. Madsen, M. Lassen, and me in the group of U.L. Andersen.

Chapter 2

Phase super-resolution with classical resources

In this Chapter we show the basic idea of super-resolution phase measurement using coherent states of light, Mach-Zehnder interferometer, and homodyne detector complemented by a suitable data processing. We demonstrate theoretically as well as experimentally the interference fringe narrowing and the sensitivity scaling according to the SNL.

2.1 Theory

The proposed super-resolution method follows the standard interferometric scheme as illustrated in Fig. 1 (a). A coherent state of light, $|\alpha\rangle$, with amplitude $\alpha > 0$ and mean photon number $N = \alpha^2$ enters the interferometer at the input balanced beam splitter described by the unitary \hat{B} ,

$$\hat{B}|\alpha\rangle|0\rangle = \left|\frac{\alpha}{\sqrt{2}}\right\rangle\left|\frac{\alpha}{\sqrt{2}}\right\rangle. \quad (2.1)$$

The resulting state acquires a phase shift, ϕ , in one arm of the interferometer, and the final state at the output is produced by interference at the second balanced beam splitter,

$$|\Psi(\phi)\rangle = \hat{B}\left|e^{i\phi}\frac{\alpha}{\sqrt{2}}\right\rangle\left|\frac{\alpha}{\sqrt{2}}\right\rangle = |\cos(\phi/2)\alpha\rangle|\sin(\phi/2)\alpha\rangle. \quad (2.2)$$

The coherent states at the outputs of the interferometer follow circular paths in the phase space (x, p) as depicted on the insets of Fig. 1 (a).

The observed phase resolution and sensitivity crucially depend on how this output state is detected. By describing the detection process with a measurement operator $\hat{\Pi}$,

the response function of the setup is the mean value of that operator, $\langle \hat{\Pi} \rangle$. Using, for example, a common intensity detector described by the observable $\hat{\Pi} = \hat{N}$, the detector response is given by

$$\langle \hat{N} \rangle = \langle \Psi(\phi) | \hat{N} | \Psi(\phi) \rangle = N \cos^2(\phi/2), \quad (2.3)$$

which is an oscillating function with a period of $\lambda/2$, thus coinciding with the standard resolution limit. The resolution can be characterized by the full-width at half maximum (FWHM) of the response function which for the standard intensity detector is $\text{FWHM} \propto \pi$.

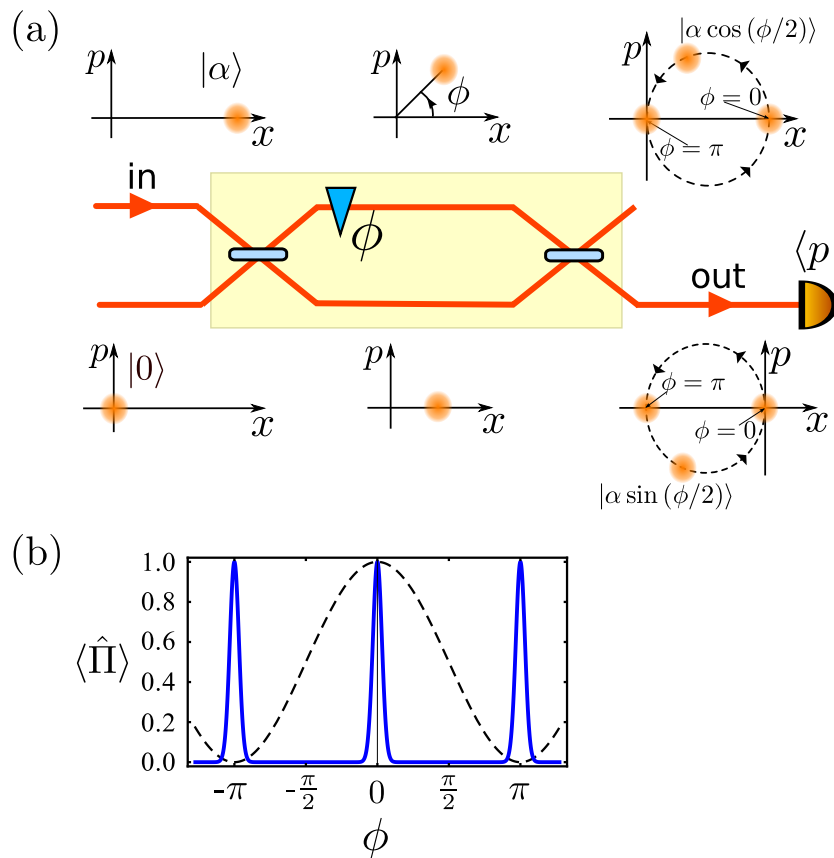


Figure 1: (a) Schematic of the experimental setup. A product of a coherent state, $|\alpha\rangle$, and a vacuum state, $|0\rangle$, is transformed through an interferometer and measured with a homodyne detector described by the ideal projector $\langle p |$. The evolutions in phase space of the two states are illustrated by the insets. (b) The phase response function $\langle \hat{\Pi} \rangle$ for the standard interferometer scheme (dashed curve) and for the super-resolving scheme (solid curve).

To beat the standard Rayleigh resolution limit, a special homodyne detector is used in replacement of the intensity detector. A homodyne detector measures the eigenvalues

of a quadrature operator $\hat{x} \cos \theta + \hat{p} \sin \theta$, where θ is the phase of the local oscillator intrinsic to the detector; \hat{x} and \hat{p} are the canonically conjugated amplitude and phase quadrature operators related to the bosonic field operator, $\hat{a} = \hat{x} + i\hat{p}$, and obey the commutation relation $[\hat{x}, \hat{p}] = i/2$. The main idea of our approach is to measure the phase quadrature \hat{p} (setting the phase of the local oscillator to $\pi/2$) and subsequently divide the measurement outcomes into two bins associated with $|p| \leq a$ and $|p| > a$. Such a measurement strategy is described by the two projectors

$$\hat{\Pi}_0 = \int_{-a}^a dp |p\rangle\langle p|, \quad \hat{\Pi}_1 = \hat{I} - \hat{\Pi}_0 \quad (2.4)$$

and the measurement observable can thus be written as

$$\hat{\Pi} = \sum_{k=1,2} \lambda_k \hat{\Pi}_k, \quad (2.5)$$

where $\lambda_0 = 1/\text{erf}(\sqrt{2}a)$ and $\lambda_1 = 0$ are the values associated with the two measurement outcomes. The detector response function $\langle \hat{\Pi} \rangle$ of this dichotomic strategy is

$$\langle \hat{\Pi} \rangle = \langle \Psi(\phi) | \hat{\Pi} | \Psi(\phi) \rangle = \frac{1}{\text{erf}(\sqrt{2}a)} \int_{-a}^a dp |\langle \sqrt{N} \cos(\phi/2) | p \rangle|^2. \quad (2.6)$$

Let us discuss first the idealized case of $a \rightarrow 0$, corresponding to binning the results for which $p = 0$ and $p \neq 0$. The mean value of the detection operator $\hat{\Pi} = |p = 0\rangle\langle p = 0|$ yields the response

$$\langle \hat{\Pi} \rangle = \exp\left(-\frac{1}{2} N \sin^2 \phi\right), \quad (2.7)$$

which is illustrated in Fig. 1 (b). FWHM of this fringe is

$$\text{FWHM} = 2 \arcsin \sqrt{(2 \ln 2)/N} \quad (2.8)$$

and by comparing it to the FWHM of the fringe associated with a standard Rayleigh limited intensity detection system, we see that super-resolution is obtained for $N > 2 \ln 2$, and for $N \rightarrow \infty$ we find a $1/\sqrt{N}$ improvement of the resolution with respect to the Rayleigh limit. Let us note that for $a \rightarrow 0$, the operator $\hat{\Pi}_0$ corresponds to the projection on the eigenstate $|p = 0\rangle$ that can be associated with the projection onto squeezed vacuum state in the limit of infinitely high squeezing parameter r ,

$$|p = 0\rangle = \lim_{r \rightarrow \infty} \frac{1}{\sqrt{\cosh r}} \sum_k \left(\frac{\tanh r}{2}\right)^k \frac{\sqrt{2k!}}{k!} |2k\rangle, \quad (2.9)$$

which is somewhat reminiscent of one of the projectors of a parity measurement [27, 32, 40].

In addition to being super-resolving, our approach also exhibits a phase sensitivity at the SNL. The sensitivity is defined as

$$\Delta\phi = \frac{\Delta\Pi}{\left|\frac{d\langle\hat{\Pi}\rangle}{d\phi}\right|} \quad (2.10)$$

and by inserting eq. (2.7), we find

$$\Delta\phi = \sqrt{\frac{2\sqrt{2\pi} \left(e^{\frac{N}{2}\sin^2\phi} - \sqrt{\frac{2}{\pi}} \right)}{N^2 \sin^2(2\phi)}}. \quad (2.11)$$

The sensitivity reaches its minimum

$$\Delta\phi_{\min} = \sqrt{\sqrt{\frac{\pi}{2}} \frac{e^{\frac{1}{4}(2+N-\sqrt{4+N^2})} - \sqrt{\frac{2}{\pi}}}{\sqrt{4+N^2}-2}} \quad (2.12)$$

near the phase points

$$\phi_{\min} = \pm \arccos \left(\sqrt{\frac{1}{2} - \frac{1}{N} + \frac{\sqrt{4+N^2}}{2N}} \right) \quad (2.13)$$

corresponding to the maximum of the derivative in the denominator of (2.10). For mean photon number $N \rightarrow \infty$ the sensitivity approaches the limit of

$$\Delta\phi_{\min} = \frac{\sqrt{\sqrt{\frac{e\pi}{2}} - 1}}{\sqrt{N}} \approx \frac{1.03}{\sqrt{N}}, \quad (2.14)$$

thus being close to the SNL. Actually, the remaining 3% discrepancy is effectively equivalent to a 3% loss or detector inefficiency—the sensitivity $1/\sqrt{N}$ would be reached using a coherent state with 3% higher amplitude.

In the limit of $a \rightarrow 0$ the measurement is not physically sound as it requires infinitely high energy. However, both the resolution and sensitivity properties are preserved even for a finite value of a . Indeed, for a general value of a the response function can be evaluated as

$$\langle\hat{\Pi}\rangle = \frac{1}{2\text{erf}(\sqrt{2}a)} \left[\text{erf}(\sqrt{2}g_-) + \text{erf}(\sqrt{2}g_+) \right], \quad (2.15)$$

where $g_{\pm} = a \pm \frac{1}{2}\sqrt{N}\sin\phi$ and $\text{erf}(\cdot)$ denotes the error function. The response function and its width are illustrated by the solid curves in Fig. 5 (a) and (c) for two different mean photon numbers. The scaling of the response width is again found to be

$$\text{FWHM} \propto \frac{1}{\sqrt{N}}. \quad (2.16)$$

Finally, the sensitivity for a finite a reads

$$\Delta\phi = \sqrt{\frac{\pi}{2} \frac{e^{(2a+\sqrt{N}\sin\phi)^2} k(2-k)}{N \cos^2\phi (e^{4a\sqrt{N}\sin\phi} - 1)^2}}, \quad (2.17)$$

where $k = \text{erf}(\sqrt{2}g_-) + \text{erf}(\sqrt{2}g_+)$. For $a = 1/2$ and $N \gg 1$ the sensitivity follows the SNL scaling,

$$\Delta\phi_{\min} \approx \frac{1.37}{\sqrt{N}}. \quad (2.18)$$

Here we pay the price for super-resolution of about 37% of coherent amplitude by which the sensitivity is effectively worsened. As in the case of $a \rightarrow \infty$, the imperfection is effectively equivalent to the loss or detector inefficiency and we can overcome it by a suitable increase of coherent state amplitude. The value of $a = 1/2$ represents a trade-off between the sensitivity and resolution. For higher value of a the sensitivity is closer to the exact SNL bound but the resolution FWHM increases and vice versa.

2.2 Multiple-fringe phase super-resolution

As we have now seen, the binary binning of quadrature measurements leads to a narrowing of the interference fringe. However, the number of fringes in an 2π period remains unchanged as opposed to interferometry with NOON states where the number of fringes increases with the photon number. It is, however, also possible with coherent states to increase the number of fringes in a period by employing a multiple binning approach instead of the binary binning strategy described above. Continuous quadrature measurement outcomes are discretized into several bins described by the projectors

$$\hat{\Pi}_k = \int_{b_k-a}^{b_k+a} |p'\rangle\langle p'| dp', \quad \hat{\Pi}_{n+1} = \hat{I} - \sum_{k=1}^n \hat{\Pi}_k. \quad (2.19)$$

This corresponds to dividing the outcomes into n equidistant intervals with width $2a$. By setting the eigenvalues $\lambda_k = 1/\text{erf}(\sqrt{2}a)$ for $k \in \{1, \dots, n\}$ and $\lambda_{n+1} = 0$, we find

the resulting response function

$$\begin{aligned} \langle \hat{\Pi} \rangle &= \sum_{k=1}^{n+1} \lambda_k \langle \mathbf{\Pi}_k \rangle = \\ &= \frac{1}{2\text{erf}(\sqrt{2}a)} \sum_{k=1}^n \left\{ \text{erf} \left[\sqrt{2}(g_- - b_k) \right] + \text{erf} \left[\sqrt{2}(g_+ + b_k) \right] \right\}, \end{aligned} \quad (2.20)$$

where b_k is the central position of the intervals on the p-quadrature line. If the distance among the intervals is $b > 2a$, the projectors are orthogonal and we can straightforwardly find the variance

$$\langle \Delta \hat{\Pi}^2 \rangle = \langle \hat{\Pi} \rangle \left(\frac{1}{\text{erf}(\sqrt{2}a)} - \langle \hat{\Pi} \rangle \right) \quad (2.21)$$

and thus the sensitivity (2.10).

2.3 Experimental realization in pulse regime

We implement the phase super-resolution protocol using attenuated pico-second pulses from Ti-sapphire laser Tiger-PS by Time-Bandwidth Products with repetition rate of 815 kHz and central wavelength of 830 nm spatially filtered by a single mode fiber. The coherent beam is divided at a highly unbalanced beam splitter consisting of half-wave plate (HWP) and polarizing beam splitter (PBS) and further attenuated by neutral density filters and another polarization attenuator, see Fig. 2 This signal with a controllable mean photon number is sent through a balanced Michelson interferometer (MI) in which the relative phase ϕ is continuously varied by a piezo driven mirror. The phase quadrature of the interferometer output state is then measured with a high-efficiency homodyne detector (HD). It is based on overlapping the output state with the reference laser mode—local oscillator with relative phase set to $\pi/2$. The output intensity is measured by two photodiodes (Hamamatsu S3883), the resulting photocurrents are subtracted and the difference signal is amplified, shaped, and acquired by an oscilloscope. The photo of the experimental setup is shown in Fig. 3

The interference contrast of the MI has a visibility level of 99.5%, the interference between the signal and the local oscillator of the HD exceeds a visibility of 98.5% and the total efficiency of the HD reaches $\eta = 90\%$. It means that the MI phase ϕ was effectively probed by a coherent state with the amplitude of approximately 5% higher. We follow the general practice and do not rescale accordingly the amplitude of the coherent state in the presented experimental results or, equivalently, we consider

an ideal detector. The mean photon number N is estimated by directing the input signal (bypassing the MI interferometer) to the homodyne detector and measuring the amplitude α of the state ($N = |\alpha|^2$). The reading is calibrated against the vacuum trace (shot noise).

The homodyne detector was custom-built for single-photon subtraction from squeezed light [37] using the Amptek-based charge-sensitive design [38] with some minor changes, particularly a better bias filtering and balancing. The detector exceeds 30 dB signal-to-noise ratio for several tens μW of local oscillator power and works very stable at 25 dB for 20 μW local oscillator with repetition rate of 815 kHz (100×10^6 photons per pulse), see Fig. 4. The electronic bandwidth of the detector spans the interval from approximately 100 Hz to 2 MHz. For the super-resolution experiment in pulse regime the parameters of the homodyne detector were modified slightly to reach higher dynamic range, which enabled us to measure the signals with high mean number of photons ($N > 100$). The modified detector possesses the gain of 0.462 mV^2 per 10^6 photons in a pulse of the local oscillator and the electronic noise of 0.498 mV^2 .

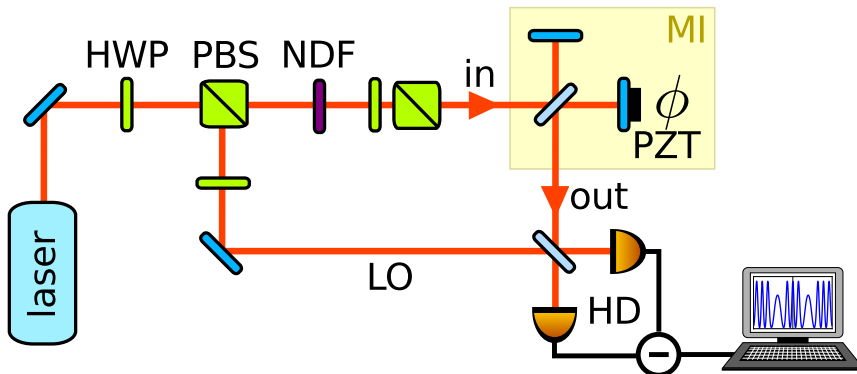


Figure 2: Experimental setup. Light from a pico-second pulsed Ti:Sapphire laser operating at 830 nm and with a repetition rate of 815 kHz is controllably divided into two beams using a half-wave plate (HWP) and a polarizing beam splitter (PBS) thereby creating a signal and a local oscillator (LO) beam for homodyne detection (HD). The power of the signal beam is controlled by a neutral density filter (NDF), a HWP and a PBS, and subsequently sent into a Michelson interferometer (MI). A piezo-crystal (PZT) attached to one of the interferometer mirrors scans the phase, ϕ , and the resulting output is measured by means of homodyne detection (HD).

2.4 Experimental results and discussion

We subject the homodyne detector outcomes to the binning procedure with the interval set to $a = 1/2$. This value is chosen as a good compromise for obtaining significantly



Figure 3: Photo of the experimental setup.

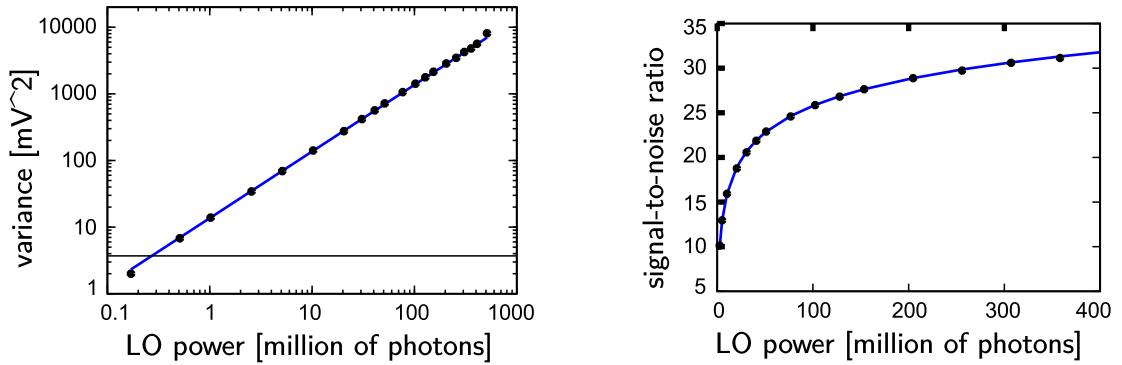


Figure 4: Linearity (a) and signal-to-noise ratio (b) of the time-domain homodyne detector. Black points represent the measured data, blue solid line (linearity) and logarithmic curve (signal-to-noise ratio) show the corresponding theoretical model, and the black solid line represents the electronic noise level.

high super-resolution and sensitivity performance close to the quantum limit. The experiment is repeated 400 times for each realization of a phase value, and the frequencies at which the measurement outcomes fall within the two quadrature intervals (described by the projectors (2.4)) are found. The resulting response functions are plotted in Fig. 5 (a)-(b) for two different power levels (red dots). A clear narrowing of the fringe with respect to the fringe for the standard approach (dashed curve) is observed, thus proving the super-resolution capabilities of our scheme [39]. We also note that the visibility of the new interference fringes is basically unchanged and close to unity. We repeat the experiment for several different mean photon numbers and the results of the FWHM are summarized in Fig. 5 (c). We also estimate the sensitivity

from the measurements and the results for two different mean photon numbers are presented by the insets of Fig. 5. These results demonstrate that the measurements possess a phase sensitivity very close to the SNL (dashed line) for certain phases. In Fig. 5 (d) we present a summary of the optimal phase sensitivities for several different mean photon numbers and compare it to the SNL (dashed curve).

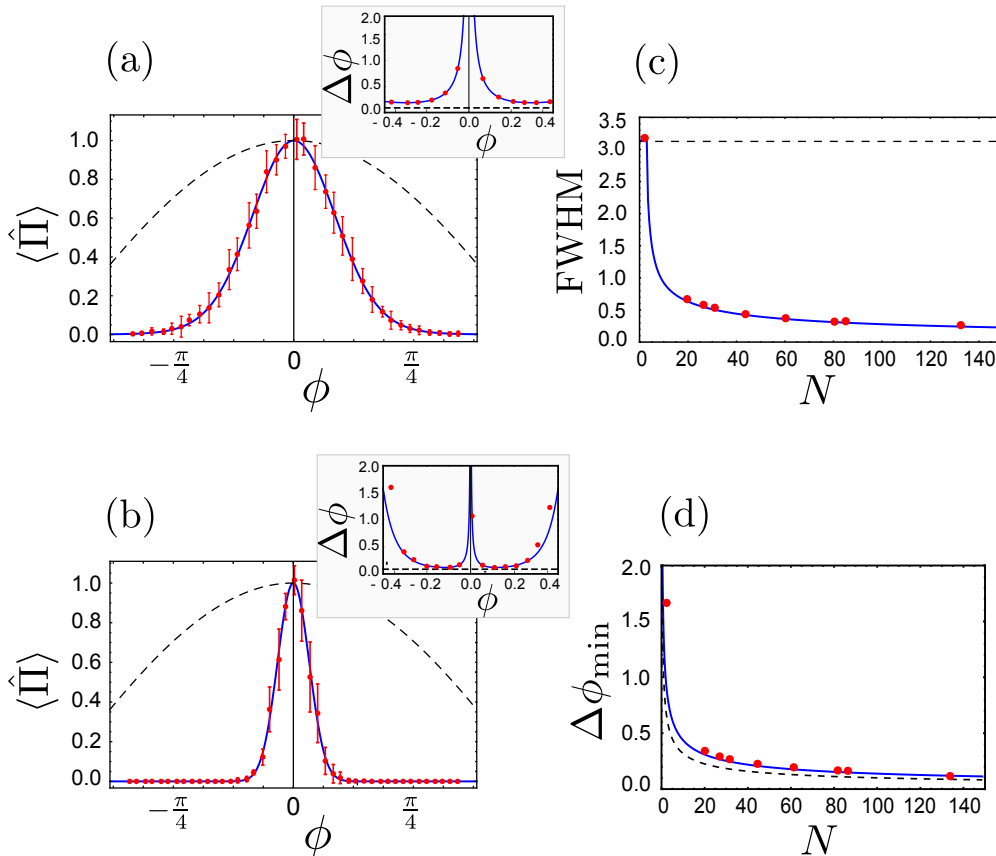


Figure 5: Performance of the super-resolving interferometer. (a) and (b) show the experimental results (dots) and the theory (solid curve) for the response function with $a = 0.5$ for two different mean photon numbers $N = 19$ and $N = 132$, respectively. The dashed curves represent the standard Rayleigh limited strategy. The insets of (a) and (b) are the results of the sensitivity as a function of ϕ for the same values of N . The dashed curves represent the SNL. (c) The resolution in terms of FWHM of our scheme as a function of the mean photon number (red dots) together with theory for our approach (solid blue curve) and for Rayleigh limited strategy (dashed line). (d) Minimum value of the sensitivity for our scheme for different mean photon numbers (red dots). The solid blue curve represents the theoretical curve, $\Delta\phi_{\min} \approx 1.37/\sqrt{N}$, and the dashed line stands for the SNL. Error bars of (c), (d) and the insets are smaller than the data points.

Using multiple binning as opposed to binary one, we demonstrate multiple fringes within one period. An example is shown in Fig. 6 for $M = 8$ fringes per period

obtained by binning the measurement outcomes along 5 intervals for a coherent state with $N = 139$ and the window width of $a = 1/2$. The central points of these intervals are located at $p = b \cdot k$ where $k \in [-2, -1, 0, 1, 2]$ and $b = 3.17$. The average fidelity of all fringes within a period is 95%.

The multiple fringe approach gives rise to a slightly lower visibility of the interference fringes, thus rendering a trade-off between the number of fringes within a period and the visibility of the resulting pattern for a given average photon number. This means that the phase sensitivity of the multi fringe approach operates at the SNL (like the two bin approach) as long as the number of fringes is adjusted according to the mean number of photons. For a fixed number of photons N , the number of fringes M depends on the choice of the parameter b as well as on the required visibility. For a given set of N , M and a there is an optimal value of b that maximizes the visibility. Fig. 7 reports two examples of the number of fringes as a function of the number of photons for two different visibilities. In this example, for each N , b has been chosen such as to maximize M and to keep the visibility above 95% or above 90%. It is clear that for higher visibility the number of fringes for a given N is lower. The points in the figure are evaluated numerically and the curves are fits that scale as $M \propto \sqrt{N}$.

In the above investigations we have considered only the measurement of the phase quadrature among all other quadratures. For the binary binning approach, this is indeed the optimal quadrature measurement (for the input state considered in Fig. 1 (a)) although super-resolution with reduced quality can be also obtained for any other quadrature measurement. This is clearly seen from the results of the multiple-binning approach in Fig. 9 which shows that the fringes are narrowest at $\phi = 0$ and broadest at $\phi = \pi/2$ effectively corresponding to a phase and an amplitude quadrature measurement, respectively. The fact that super-resolution can be obtained for any quadrature measurement suggests that we may relax the stringent phase reference in our homodyne detector thus measuring a random quadrature and thereby attaining super-resolution with a simplified strategy.

Furthermore, the performance of our method is basically unaltered in the presence of loss since the loss can be ideally compensated by increasing the mean number of photon of the input state, which is the benefit of using only classical states and classical detector. For example, for 50% transmittance of the sample it is sufficient to increase the intensity of the coherent state by factor of two to completely recover super-resolution as well as the sensitivity, whereas such the loss would be highly detrimental for a measurement employing nonclassical light and, particularly, the NOON states.

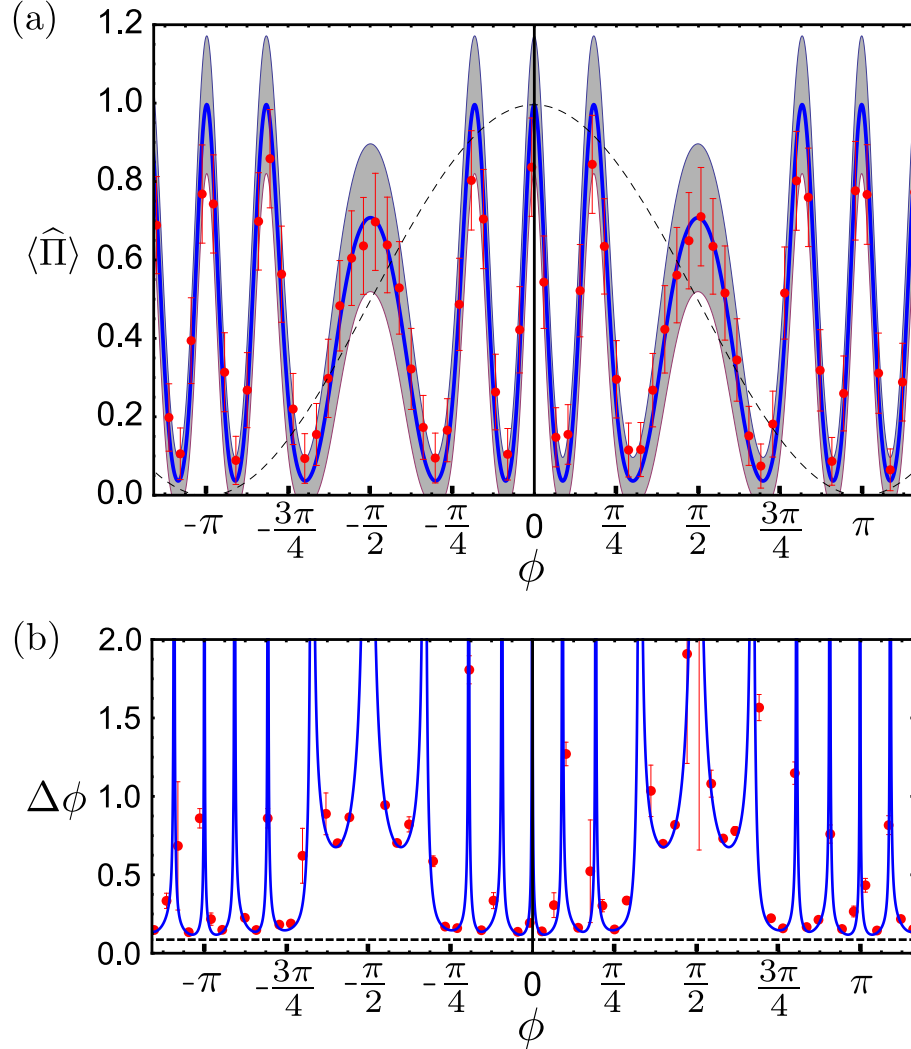


Figure 6: Results for the multiple binning approach. (a) Response function with 8 fringes per period for a coherent state with $N = 139$. The average fidelity of all fringes within a period is 95%. The data (red dots) fit well with theory (blue line) and the uncertainty for each point lies inside the theoretically predicted uncertainty, represented by the shaded area. Interference fringe corresponding to the Rayleigh limited approach is shown by the dashed curve. (b) Phase sensitivity for the multiple binning approach associated with the experimental results (dots) and the theory (solid curve). Near SNL performance (represented by the dashed line) is obtained for several phases.

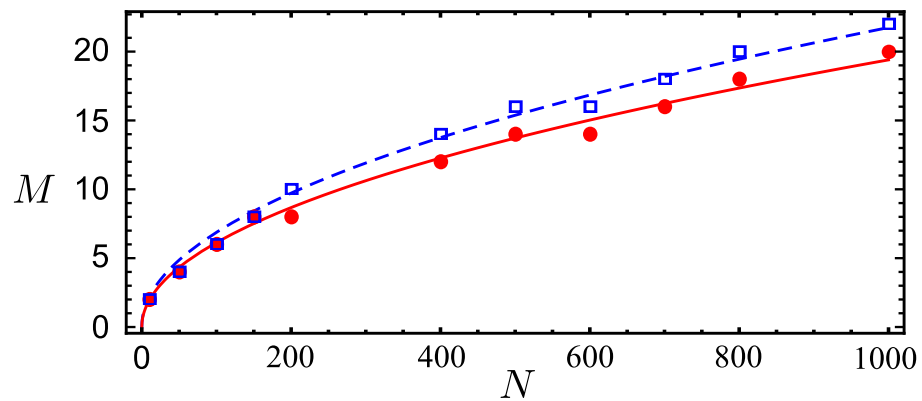


Figure 7: Plot of the number of fringes M for which the visibility is larger than 0.95 (red solid trace and dots) and 0.90 (blue dashed trace and squares) as a function of the average photon number, N , of the coherent state. The dots and squares correspond to numerical estimates whereas the curves are theoretical fits.

Chapter 3

Phase super-resolution beyond shot noise level with coherent and squeezed states

Using squeezed states of light in addition to coherent states, we are able to improve the sensitivity of the super-resolution measurement scheme to be exactly at or even beyond the shot noise limit. The phase can be measured in super-resolving and super-sensitive regime which was thought to be possible only using quantum non-Gaussian states, e.g. NOON states. The obvious drawback of this extension is twofold: first, the increased sensitivity to optical losses; and second, more stringent requirements for local oscillator phase stability. Thus, the squeezed light injection is suitable for purely phase samples and low loss measurement setups. In this Chapter, we derive the basic theoretical description, show the limitations, and demonstrate preliminary experimental test of the method.

3.1 Theory

The presented measurement scheme follows Caves' proposal [33] where the squeezed vacuum is injected into an unused input port of the interferometer, see Fig. 8. The input state of optical signal described by the Wigner function

$$W_{\text{in}}(x_1, p_1, x_2, p_2) = W_{|\alpha\rangle}(x_1, p_1)W_{|r\rangle}(x_2, p_2) = \frac{2e^{-2((x_1-\alpha)^2+p_1^2)}}{\pi} \cdot \frac{2qe^{-2\left(q^2s^2x_2^2+\frac{p_2^2}{s^2}\right)}}{\pi} \quad (3.1)$$

enters the interferometer with the phase shift ϕ in one arm. Here α is amplitude of the coherent state, $s = e^{-r}$, where r denotes the squeezing parameter, and q represents the

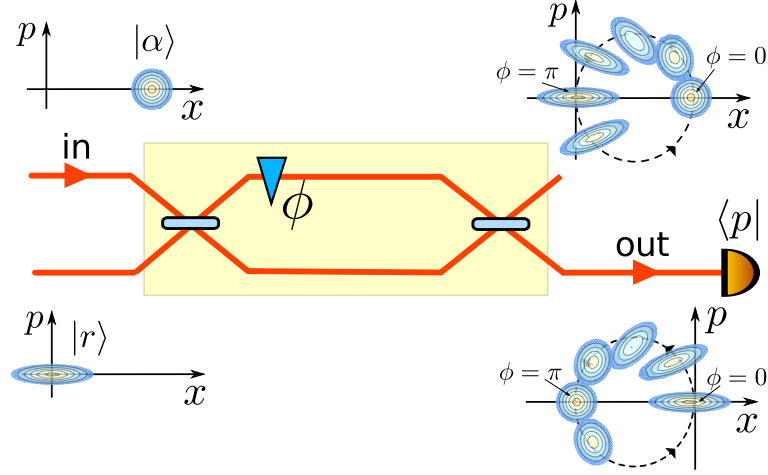


Figure 8: A product of a coherent state, $|\alpha\rangle$, and a squeezed vacuum state, $|r\rangle$, is transformed through an interferometer and measured with a homodyne detector. The evolution in phase space is illustrated by the insets.

purity of the squeezed state. One output port of the interferometer is not observed, thus traced out. The Wigner function at the remaining port,

$$\begin{aligned}
 W(x, p) = & \frac{4s}{\pi \sqrt{(s^2 + 1)^2 - (s^2 - 1)^2 \cos^2(\phi)}} \exp \left(\left[2((s^2 + 1)(\alpha^2 + 2p \sin \phi(\alpha - s^2 x + x) + \right. \right. \\
 & 2\alpha x + (s^2 + 1)(p^2 + x^2)) + (s^2 - 1) \cos^2 \phi (\alpha^2 + 2\alpha x - (s^2 + 1)(p - x)(p + x)) - \\
 & \left. \left. 2 \cos \phi (p(s^2 - 1) \sin \phi (\alpha + s^2 x + x) + s^2(\alpha - s x + x)(\alpha + s x + x) + p^2(s^2 - 1)) \right] / \right. \\
 & \left. \left[(s^2 - 1)^2 \cos^2(\phi) - (s^2 + 1)^2 \right] \right), \quad (3.2)
 \end{aligned}$$

evolves around the similar circular path in the phase space (x, p) as in the case of input coherent state only. The variance of phase quadrature, however, changes from the minimum value corresponding to the squeezed state (for phase $\phi = 0$) to the maximum one corresponding to the shot noise level ($\phi = \pi$). The total mean number of photons employed is

$$\langle \hat{N} \rangle = \frac{1}{4} \left(\frac{1}{q^2 s^2} + s^2 + 4|\alpha|^2 - 2 \right) = \alpha^2 + \sinh^2(r). \quad (3.3)$$

In the idealized case of $\hat{\Pi} = |p=0\rangle\langle p=0|$ measurement ($a \rightarrow 0$) and pure input state ($q = 0$) the response

$$\langle \hat{\Pi} \rangle = \frac{2\sqrt{2}s^2 \exp \left(-\frac{2s^2 x^2 \sin^2 \phi}{(s^2 - 1) \cos \phi ((s^2 + 1) \cos \phi + 2s^2) + (s^2 + 1)^2} \right)}{\sqrt{(s^4 - 1) \cos(2\phi) + 4(s^2 - 1) s^2 \cos \phi + 3s^4 + 4s^2 + 1}} \quad (3.4)$$

shows the $1/|\alpha|$ resolution improvement with respect to the Rayleigh bound in the limit of $|\alpha| \rightarrow \infty$. For no squeezing, $s = 0$, (3.4) coincides with (2.7). For a general value of a the response function reads

$$\langle \hat{\Pi} \rangle = \frac{1}{2\text{erf}(\sqrt{2}a/s)} \left[\text{erf} \left(\sqrt{\frac{2}{C}} g_- \right) + \text{erf} \left(\sqrt{\frac{2}{C}} g_+ \right) \right], \quad (3.5)$$

where $g_{\pm} = a \pm \frac{1}{2}|\alpha| \sin \phi$ and

$$C = \frac{q^2 s^2 (s^2(1 + \cos \phi)^2 + 2(1 - \cos \phi)) - \cos^2 \phi + 1}{4q^2 s^2}. \quad (3.6)$$

The resolution gain scaling is preserved for a finite a , fringe FWHM $\propto 1/|\alpha|$. See Fig. 9(a) for an example of the phase response function under realistic conditions of partially mixed squeezed state.

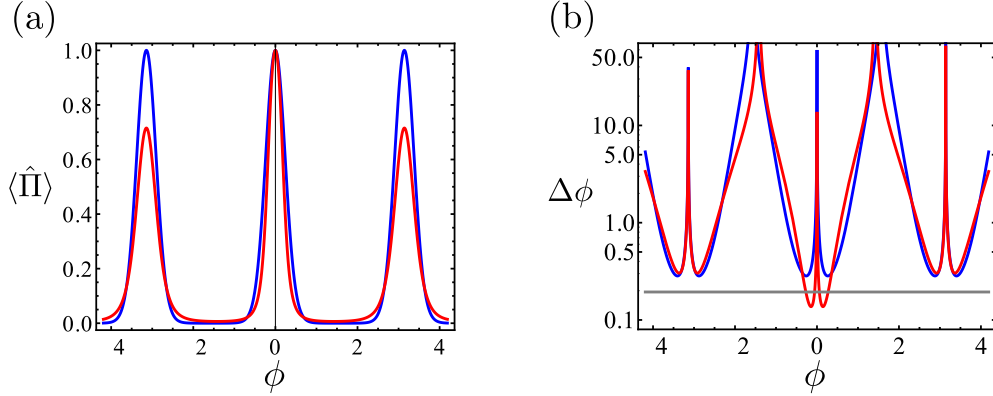


Figure 9: (a) The phase response and (b) the sensitivity of the the proposed protocol employing coherent and squeezed states and homodyne detection. The bin size is set to $a = 1/2$ and the amplitude of injected coherent state $|\alpha| = 5$. A squeezed state with squeezing of -6 dB and antisqueezing of 9 dB: $q = 0.7$, $s = 0.5$ (red) and the measurement without squeezing: $q = 1$, $s = 1$ (blue) are compared. Gray line in (b) denotes the SNL.

The variance of the measurement operator $\hat{\Pi}$ is given by Eq. (2.21) and the phase sensitivity is evaluated using Eq. (2.10),

$$\Delta\phi = \frac{\sqrt{\frac{\pi}{2}} C^{3/2} \sqrt{(2-k)k}}{e^{-\frac{2g_-^2}{C}} (C'g_- + \alpha C \cos \phi) + e^{-\frac{2g_+^2}{C}} (C'g_+ - \alpha C \cos \phi)}. \quad (3.7)$$

Here $k = \text{erf}(g_- \sqrt{2/C}) + \text{erf}(g_+ \sqrt{2/C})$ and $C' = dC/d\phi$. The sensitivity, shown in the Fig. 9(b), beats the standard quantum limit for finite range of phase values. Without squeezing, $s = 1$ and for pure state, $q = 1$, the formulas simplify ($C = 1$, $C' = 0$)

and the resolution as well as the sensitivity coincide with results obtained for classical resources, see Sec. 2.1. Particularly, the sensitivity reads

$$\Delta\phi = \frac{\sqrt{\frac{\pi}{2}}\sqrt{(2-k)k}e^{2(a+\frac{1}{2}x\sin\phi)^2}}{x\cos\phi(e^{4ax\sin\phi}-1)}. \quad (3.8)$$

Super-sensitivity multiple-fringe case can be derived as a straightforward extension of the previous theory employing the multiple binning approach in the same way as it was done in the Sec. 2.2 for coherent states.

3.2 The ultimate limit of phase sensitivity

Previous results can be compared with the original Caves' work [33] assuming the intensity detection at the output of the interferometer. Contrary to our homodyne detection and binarization, there is no fringe narrowing. On the other hand, the Caves' protocol allows for optimum sensitivity. The minimum attainable sensitivity reads

$$\Delta\phi_{\min} = \sqrt{\frac{s^2}{|\alpha|^2} + \frac{(\frac{1}{s}-s)^2}{4|\alpha|^4}} = \sqrt{\frac{e^{-2r}}{|\alpha|^2} + \frac{\sinh^2 r}{|\alpha|^4}}, \quad (3.9)$$

where $|\alpha| \gg |\cot(\phi/2)\sinh r|$ is assumed. For $r = \frac{1}{4}\ln(1+4|\alpha|^2)$ the sensitivity reaches its optimum of

$$\Delta\phi_{\min} = \frac{1}{\sqrt{2}} \frac{\sqrt{\sqrt{1+4|\alpha|^2}-1}}{|\alpha|^2} \quad (3.10)$$

which scales as $1/|\alpha|^{\frac{3}{2}}$ in the limit of $N \rightarrow \infty$.

The resolution of our protocol improves with increasing the coherent state amplitude. We would like to use the highest possible optical power which does not corrupt the sample and does not saturate the detector. For each amplitude, the optimum squeezing should be adjusted and then optimum value a of the bin size and the phase with best sensitivity should be found. However, the optimum squeezing required is of about 13 dB already for $|\alpha| = 10$ and increases quickly. Taking into account the maximum squeezing available, we can fix this particular value and run the optimization only for parameters a and ϕ . For example, having the squeezing of -4 dB and antisqueezing of 8 dB, $s = 0.63$ and $q = 0.63$, the optimum value of a depends slightly on the amplitude. For the range of $|\alpha| \in [3, 21]$, it lies within the interval of $a \in [0.524, 0.587]$ which is close to $1/2$. The best attainable sensitivity of our protocol is shown in the Fig. 10 and compared with the SNL and Caves' ultimate bound.

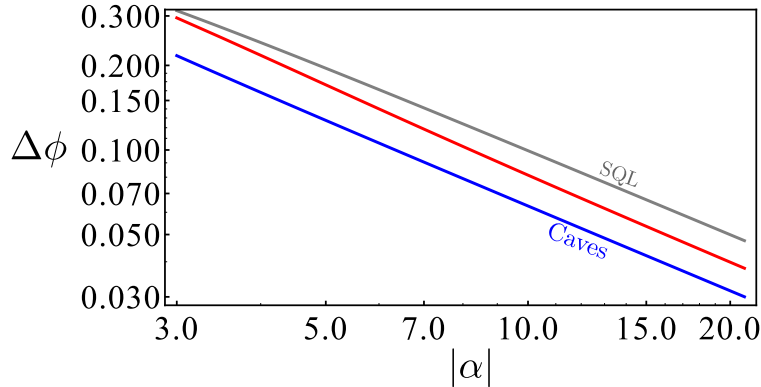


Figure 10: The sensitivity of the super-resolving protocol using -4 dB of squeezing with purity of 63% (antisqueezing of 8 dB) as a function of the coherent state amplitude (red). The bin size a as well as the phase ϕ are optimized for the best sensitivity for each amplitude $|\alpha|$. Our protocol is compared with the SNL (gray) and with Caves' minimum sensitivity (blue). Both the limits are correctly evaluated using the total mean number of photons, including the squeezing contribution.

3.3 Preliminary experimental test in continuous-wave regime

Quantum states of light, coherent and squeezed, are prepared at 4.9 MHz sideband of a continuous-wave optical carrier signal with the central wavelength of 1064 nm. The amplitude squeezing is generated by means of optical parametric oscillator with periodically poled KTP crystal placed in bow-tie cavity pumped by the second harmonic of the fundamental wavelength. The detected squeezing variance exceeds 3 dB. The coherent state is prepared by electro-optic modulator and its amplitude is adjusted by a power of radio-frequency driving signal. The modulation is locked to the antisqueezing direction.

The measurement interferometer is implemented in polarization degree of freedom using waveplates and polarizing beam splitters. Two copropagating orthogonal polarization modes acquire the relative phase proportional to the angle of the waveplate placed in between of the polarizing beam splitters [41].

The continuous-wave homodyne detector at the output port of the interferometer projects the signal to the phase quadrature. The homodyne electronic signal is then down mixed from 4.9 MHz to DC, low passed with approximately 90 kHz, and sampled at 500 kHz by analog-to-digital converter card in personal computer. The quadrature data are processed and binarized using the same method as in the pulsed experiment described in the previous chapter.

The resulting phase response and sensitivity for two values of mean number of photons, $N = 7.24$ and $N = 50.4$, are shown in the Fig. 11. We can clearly observe the narrowing of the fringe similar to the measurement using only coherent states. However, the small noise penalty (2.18) we have to pay for the super-resolution is compensated here by a lower variance of the employed squeezed light. Actually, the squeezing level is high enough to demonstrate super-sensitivity for sufficiently strong coherent state. Indeed, for the total mean number of photons $N = 50.4$ the sensitivity goes beyond SNL for several phases.

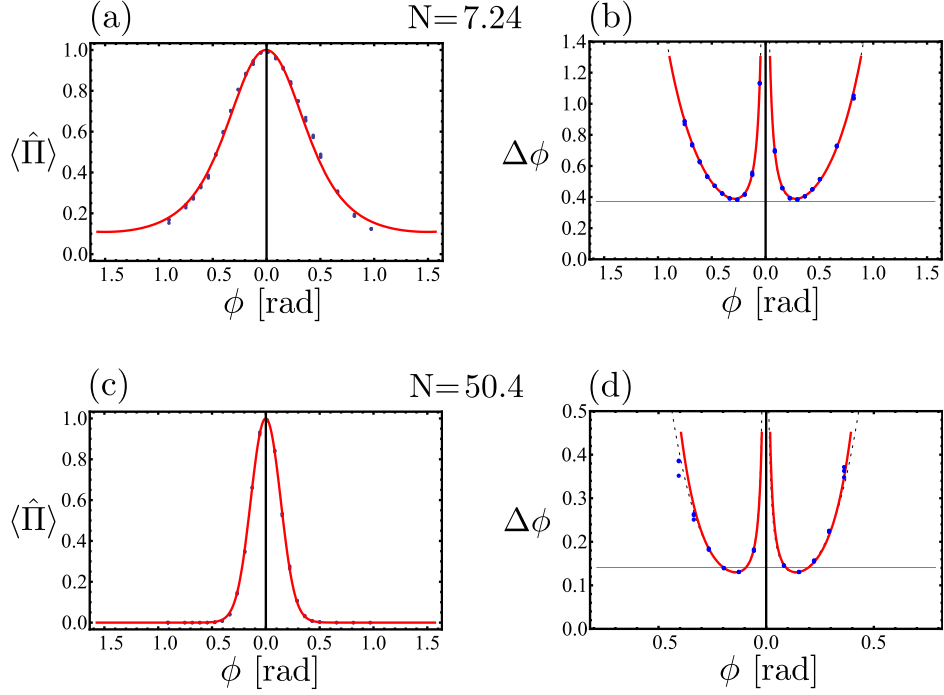


Figure 11: The phase response (a,c) and sensitivity (b,d) of our measurement (blue circles) and the corresponding theoretical model (solid red curve) shown for two distinct values of mean number of photons. The least-square fit of the sensitivity (dashed black curve) is plotted for the comparison. Statistical uncertainty is comparable with the size of data symbol.

Chapter 4

Conclusion

In the Thesis we have shown surpassing the Rayleigh resolution limit using only classical resources while keeping the sensitivity close to the SNL. The theory as well as the experimental verification have been presented. We have discussed the connection between resolution and sensitivity. Furthermore, we have applied squeezed light to push the sensitivity beyond the SNL.

More specifically, in the first part of this Thesis, we have demonstrated the narrowing of an optical phase response function and compression of interference fringes by factor of \sqrt{N} with the sensitivity scaling $1/\sqrt{N}$ employing coherent states of light and homodyne measurement. Both the phase resolution and the phase sensitivity was found to scale inversely with the coherent state amplitude.

In contrast to the previous super-resolution schemes based on NOON states or photon counters, the measurement presented here is intrinsically deterministic. It means that we keep every single measurement outcome and do not perform a post selection of the outcomes to extract the desired super-resolving feature as done in previous implementations [12–15, 26, 28, 41]. Due to this common post selection procedure, which significantly reduces the number of available resource states, all these experiments exhibit a phase sensitivity that is lower than the one obtained here if the actual number of photons passing through the sample is taken into account. Likewise, the resolution of previous implementations is practically limited by the number of entangled photons in the NOON state or by the number of photons that can be resolved in a photon counter, both of which are presently limited to approximately eight. Using the scheme outlined here the resolution limit can in practice be arbitrarily small. For example, using 1 pW of visible laser radiation, we find a FWHM phase resolution of the order of 0.1 nm. A similar resolution can be obtained by using an experimentally unfeasible 500 photon NOON state. Moreover, using such a state in the presence of just 0.2% loss, it is impossible to attain sensitivity operation at the SNL due to the extreme fragility

of high NOON states [18]. In contrast, the performance of our method is basically unaltered in the presence of loss since the loss can be ideally compensated by increasing the mean number of photon of the input state.

In the second part of the Thesis, we have found theoretically that the interferometric scheme with a squeezed state and a dichotomic homodyne detector will in addition to the super-resolving capabilities exhibit a phase sensitivity that beats the SNL. The preliminary experimental test has been presented with a significant narrowing of the interference fringe and with the sensitivity slightly below the SNL. This is the first demonstration of the super-resolution and super-sensitivity measurement using only Gaussian resources: the coherent and squeezed states and the homodyne detector.

The work presented in this Thesis is based on the paper: E. Distante, M. Ježek, and U.L. Andersen, *Deterministic super-resolution with coherent states at the shot noise limit*, Phys. Rev. Lett. 111, 033603 (2013). I undertook this project during my postdoc in the group of prof. U.L. Andersen at Technical University of Denmark in 2009-2010. Simultaneously, I co-supervised the Master's theses *Super-resolution with coherent states* by E. Distante, which was successfully defended at Università degli Studi di Milano in 2011. The theory in the second part of the Theses (squeezed states) has been done by me, the preliminary experimental test was performed by L.S. Madsen, M. Lassen, and me in the group of U.L. Andersen.

Bibliography

- [1] M. Born, E. Wolf, Principle of Optics (Cambridge University Press, 1999).
- [2] M. Bertero and P. Boccacci, Introduction to Inverse Problems in Imaging (IOP Publishing, 1998).
- [3] J. K. Seo and E. J. Woo, Nonlinear Inverse Problems in Imaging (Wiley, 2013).
- [4] M. Ježek and Z. Hradil, Reconstruction of spatial, phase and coherence properties of light, *J. Opt. Soc. Am. A* **21**, 081407 (2004).
- [5] M. Dyba and S.W. Hell, Focal spots of size $\lambda/23$ open up far-field fluorescence microscopy at 33 nm axial resolution, *Phys. Rev. Lett.* **88**, 163901 (2002); E. Ritweger, et al., STED microscopy reveals crystal colour centres with nanometric resolution, *Nat. Phot.* **3**, 144-147 (2009).
- [6] J.J. Bollinger, W.M. Itano, D.J. Wineland, and D.J. Heinzen, Optimal frequency measurements with maximally correlated states, *Phys. Rev. A* **54**, R4649(R) (1996).
- [7] A.N. Boto, P. Kok, D. Abrams, S. Braunstein, C. Williams, and J. Dowling, Quantum interferometric optical lithography: exploiting entanglement to beat the diffraction limit, *Phys. Rev. Lett.* **85**, 2733 (2000).
- [8] D. Leibfried, et al., Creation of a six-atom Schrödinger cat state, *Nature* **438**, 639 (2005).
- [9] J.A. Jones, S.D. Karlen, J. Fitzsimons, A. Ardavan, S.C. Benjamin, G.A.D. Briggs, and J. J. L. Morton, Magnetic field sensing beyond the standard quantum limit using 10-spin NOON states, *Science* **324**, 1166 (2009).
- [10] Y.-A. Chen, X.-H. Bao, Z.-S. Yuan, S. Chen, B. Zhao, and J.-W. Pan, Heralded Generation of an Atomic NOON State, *Phys. Rev. Lett.* **104**, 043601 (2010).

- [11] J.G. Rarity, P.R. Tapster, E. Jakeman, T. Larchuk, R.A. Campos, M.C. Teich, and B.E.A. Saleh, Two-photon interference in a Mach-Zehnder interferometer, *Phys. Rev. Lett.* **65**, 1348 (1990).
- [12] M.W. Mitchell, J.S. Lundeen, and A.M. Steinberg, Super-resolving phase measurements with a multiphoton entangled state, *Nature* **429**, 161 (2004).
- [13] P. Walther, J.-W. Pan, M. Aspelmeyer, R. Ursin, S. Gasparoni, and A. Zeilinger, De Broglie wavelength of a non-local four-photon state, *Nature* **429**, 158 (2004).
- [14] Nagata, T. et al. T. Nagata, R. Okamoto, J.L. O'Brien, K. Sasaki, and S. Takeuchi, Beating the standard quantum limit with four-entangled photons, *Science* **316**, 726 (2007).
- [15] I. Afek, O. Ambar, and Y. Silberberg, High-NOON states by mixing quantum and classical light, *Science* **328**, 879 (2010).
- [16] V. Giovannetti, S. Lloyd, and L. Maccone, Advances in quantum metrology, *Nat. Photonics* **5**, 222 (2011).
- [17] J. Fiurášek, Conditional generation of N -photon entangled states of light, *Phys. Rev. A* **65**, 053818 (2002).
- [18] M.A. Rubin and S. Kaushik, Loss-induced limits to phase measurement precision with maximally entangled states, *Phys. Rev. A* **75**, 053805 (2007).
- [19] J.S. Toll, Causality and the dispersion relation: logical foundations, *Phys. Rev.* **104**, 1760 (1956).
- [20] U. Dorner, R. Demkowicz-Dobrzanski, B. Smith, J. Lundeen, W. Wasilewski, K. Banaszek, and I. Walmsley, Optimal quantum phase estimation, *Phys. Rev. Lett.* **102**, 040403 (2009).
- [21] B.L. Higgins, D.W. Berry, S.D. Bartlett, H.M. Wiseman, and G.J. Pryde, Entanglement-free Heisenberg-limited phase estimation, *Nature (London)* **450**, 393 (2007).
- [22] B.L. Higgins, D.W. Berry, S.D. Bartlett, M.W. Mitchell, H.M. Wiseman, and G.J. Pryde, Demonstrating Heisenberg-limited unambiguous phase estimation without adaptive measurements, *New J. Phys.* **11**, 073023 (2009).
- [23] K.L. Pagnell and D.T. Pegg, Retrodictive quantum optical state engineering, *J. Mod. Opt.* **51**, 1613 (2004).

- [24] S.J. Bentley and R.W. Boyd, Nonlinear optical lithography with ultra-high sub-Rayleigh resolution, *Opt. Express* **12**, 5735, (2004).
- [25] G. Khoury, H. Eisenberg, E. Fonseca, and D. Bouwmeester, Nonlinear Interferometry via Fock State Projection, *Phys. Rev. Lett.* **96**, 203601 (2006).
- [26] K.J. Resch, K. Pregnell, R. Prevedel, A. Gilchrist, G. Pryde, J. O'Brien, and A. White, Time-reversal and super-resolving phase measurement, *Phys. Rev. Lett.* **98**, 223601 (2007).
- [27] Y. Gao, P.M. Anisimov, C.F. Wildfeuer, J. Luine, H. Lee, and J.P. Dowling, Super-resolution at the shot noise limit with coherent states and photon-number-resolving detectors, *J. Opt. Soc. Am. B* **27**, A170 (2010).
- [28] F. Guerrieri, L. Maccone, F.N.C. Wong, J.H. Shapiro, S. Tisa, and F. Zappa, Sub-Rayleigh imaging via N photon detection, *Phys. Rev. Lett.* **105**, 163602 (2010).
- [29] C. Kothe, G. Bjork, and M. Bourennane, Arbitrary high super-resolving phase measurements at telecommunication wavelengths, *Phys. Rev. A* **81**, 063836 (2010).
- [30] H. Shin, K.-W.-C. Chan, H.J. Chang, and R.W. Boyd, Quantum spatial superresolution by optical centroid measurements, *Phys. Rev. Lett.* **107**, 083603 (2011).
- [31] L. Cohen, D. Istrati, L. Dovrat, and H.S. Eisenberg, Super-resolved phase measurements at the shot noise limit by parity measurement, *Opt. Express* **22**, 11945 (2014).
- [32] W.N. Plick, P.M. Anisimov, J.P. Dowling, H. Lee, and G.S. Agarwal, Parity detection in quantum optical metrology without number-resolving detectors, *New J. Phys.* **12**, 113025 (2010).
- [33] C.M. Caves, Quantum-mechanical noise in an interferometer, *Physical Review D* **23**, 1693 (1981).
- [34] R. Schnabel, N. Mavalvala, D.E. McClelland, and Ping K. Lam, Quantum metrology for gravitational wave astronomy, *Nat. Commun.* **1**, 121 (2010).
- [35] The LIGO Scientific Collaboration, A gravitational wave observatory operating beyond the quantum shot-noise limit, *Nat. Phys.* **7**, 962 (2011).
- [36] J. Aasi et al., Enhanced sensitivity of the LIGO gravitational wave detector by using squeezed states of light, *Nat. Photon.* **7**, 613 (2013).

- [37] A. Tipsmark, R. Dong, A. Laghaout, P. Marek, M. Ježek, and U.L. Andersen, Experimental demonstration of a Hadamard gate for coherent state qubits, *Phys. Rev. A* **84**, 050301(R) (2011).
- [38] H. Hansen, T. Aichele, C. Hettich, P. Lodahl, A. I. Lvovsky, J. Mlynek, and S. Schiller, Ultrasensitive pulsed, balanced homodyne detector: application to time-domain quantum measurements, *Opt. Lett.* **26**, 1714 (2001).
- [39] E. Distante, M. Ježek, and U.L. Andersen, Deterministic superresolution with coherent states at the shot noise limit, *Phys. Rev. Lett.* **111**, 033603 (2013).
- [40] C.C. Gerry and J. Mimih, The parity operator in quantum optical metrology, *Contemp. Phys.* **51**, 497 (2010).
- [41] G.Y. Xiang, H.F. Hofmann, and G.J. Pryde, Optimal multi-photon phase sensing with a single interference fringe, *Sci. Rep.* **3**, 2684 (2013).